Space Weather

RESEARCH ARTICLE
10.1002/2017SW001790

Key Points:
- Empirical modeling of the lower part of topside ionosphere using a combination of IRI UP method and Swarm satellite data over Europe
- Investigation of α-Chapman, β-Chapman, Epstein, and exponential analytical functions in topside modeling
- Validation against COSMIC/FORMOSAT-3 Radio Occultation profiles pointed out that the best performance is obtained for the α-Chapman function

Correspondence to:
A. Pignalberi,
alessio.pignalberi2@unibo.it

Citation:
Pignalberi, A., Pezzopane, M., & Rizzi, R. (2018). Modeling the lower part of the topside ionospheric vertical electron density profile over the European region by means of Swarm satellites data and IRI UP method. *Space Weather*, *16*, 304–320. https://doi.org/10.1002/2017SW001790

Received 4 DEC 2017
Accepted 2 MAR 2018
Accepted article online 7 MAR 2018
Published online 30 MAR 2018

Modeling the Lower Part of the Topside Ionospheric Vertical Electron Density Profile Over the European Region by Means of Swarm Satellites Data and IRI UP Method

A. Pignalberi[1], **M. Pezzopane**[2], **and R. Rizzi**[1]

[1]Dipartimento di Fisica e Astronomia, Alma Mater Studiorum-Università di Bologna, Bologna, Italy, [2]Istituto Nazionale di Geofisica e Vulcanologia, Rome, Italy

Abstract An empirical method to model the lower part of the ionospheric topside region from the *F*2 layer peak height to about 500–600 km of altitude over the European region is proposed. The method is based on electron density values recorded from December 2013 to June 2016 by Swarm satellites and on *foF*2 and *hmF*2 values provided by IRI UP (International Reference Ionosphere UPdate), which is a method developed to update the IRI model relying on the assimilation of *foF*2 and *M*(3000)*F*2 data routinely recorded by a network of European ionosonde stations. Topside effective scale heights are calculated by fitting some definite analytical functions (α-Chapman, β-Chapman, Epstein, and exponential) through the values recorded by Swarm and the ones output by IRI UP, with the assumption that the effective scale height is constant in the altitude range considered. Calculated effective scale heights are then modeled as a function of *foF*2 and *hmF*2, in order to be operationally applicable to both ionosonde measurements and ionospheric models, like IRI. The method produces two-dimensional grids of the median effective scale height binned as a function of *foF*2 and *hmF*2, for each of the considered topside profiles. A statistical comparison with Constellation Observing System for Meteorology, Ionosphere, and Climate/FORMOsa SATellite-3 collected Radio Occultation profiles is carried out to assess the validity of the proposed method and to investigate which of the considered topside profiles is the best one. The α-Chapman topside function displays the best performance compared to the others and also when compared to the NeQuick topside option of IRI.

1. Introduction

The topside ionosphere extends from the *F*2 layer peak height (*hmF*2) to the upper transition height (the height between the oxygen ion and hydrogen ion dominated plasma regions). The plasma density distribution of this region is largely determined by field-aligned plasma flows and plasma transport processes (Rishbeth & Garriott, 1969), and because of the large fraction of the total electron content (TEC) it contains, its modeling is extremely important for telecommunication's purposes.

Knowledge of the physical and chemical state of the plasma in this region is very problematic because equipment commonly used to sound the ionosphere are not able to probe it. In fact, ground-based ionosondes can only measure the bottomside part of the vertical electron density profile, up to the height (*hmF*2) of the *F*2 layer electron density peak (*NmF*2). This task requires the use of more sophisticated and expensive techniques and equipment: topside sounders, radio occultation (RO), incoherent scatter radars (ISRs), and Langmuir probes onboard low Earth orbit (LEO) satellites.

Difficulties in modeling the topside part of the ionosphere are testified by the fact that often the International Reference Ionosphere (IRI) model (Bilitza et al., 2014) does not represent properly the real features of this part of the ionosphere (Bilitza et al., 2006). For example, the first IRI topside formulation (based on the Bent model; Bilitza, 1990) tended to overestimate the electron density in the upper ionosphere (from about 500 km above the *F*2 layer peak upward) reaching a factor of about 3 at 1,000 km above the ionospheric peak height. In order to address this problem, a correction factor (varying with altitude, modified dip latitude, and local time), based on more than 150,000 topside profiles from Alouette-1, Alouette-2, International Satellites for Ionospheric Studies-1 (ISIS-1), and ISIS-2 topside sounders, was introduced in the IRI 2007 version (Bilitza, 2004). A further IRI topside option, based on the NeQuick topside formulation (Coisson et al., 2006; Radicella & Leitinger, 2001), was introduced later to improve some shortcomings (Bilitza, 2009). Despite these huge efforts, the topside modeling in IRI is still a challenge, as it was recently demonstrated by Pignalberi

et al. (2016), who made a comparison between electron density values in the topside part of the ionosphere measured by Swarm satellites and calculated by IRI.

The need to mathematically model the topside ionosphere led many scientists to apply several analytical functions to fit the sparse information in this region coming from topside sounders, ISRs, Langmuir probes in situ data, and RO data. The most used analytical functions are Chapman (Chapman, 1931), Epstein (Rawer, 1988), exponential, and parabolic functions or a linear combination of these (Kutiev & Marinov, 2007). All these formulations strongly rely on a parameter called *scale height* whose definition and calculation are the most difficult tasks in the search of the best topside formulation. In all the aforementioned functions, the scale height controls the shape of the topside profile, thus the vertical distribution of the electron density in the topside ionosphere; this is why the scale height is strongly connected with the ionospheric dynamics, plasma thermal structure, and composition (Liu, Le, et al., 2007; Liu, Wan, et al., 2007; Tulasi Ram et al., 2009). The definition of the scale height parameter depends on the analytical formulation used and on the type of data on which it is built. From a theoretical point of view the *plasma scale height* H_p is defined as $H_p = \frac{k_b T_p}{m_i g}$ (Hargreaves, 1992), where k_b is the Boltzmann constant, $T_p = T_e + T_i$ is the plasma temperature (T_e and T_i are the electron and ion temperature, respectively), m_i is the ion mean molar mass, and g is the acceleration due to gravity. However, to apply this definition, one should know the vertical distribution of plasma temperature and that of each ion constituent, which is difficult. This is why more practical approaches based directly on electron density measurements are instead used. With regard to this, the *effective scale height*, frequently called H_m in the literature (Liu, Le, et al., 2007; Liu, Wan, et al., 2007), is the parameter that can be inferred by fitting some analytical functions to electron density values. Then, the effective scale height is a mere empirical parameter which is used to fit measured data with analytical functions, in order to obtain the most reliable representation of the topside vertical electron density distribution.

This parameter can be calculated in various ways, depending on the type of available ionospheric data. Bottomside electron density values retrieved by ionosondes can be used to estimate the topside ionospheric profile approximating the *F*2 layer region and the overlying region, by an α-Chapman function with an effective scale height determined around *hmF*2 (Huang & Reinisch, 2001; Reinisch et al., 2004).

Indeed, several empirical methods exploit topside ionosphere retrieved data. Some of these are based on topside sounders flown from 1960s to 1980s, such as Alouette-1 and Alouette-2, ISIS-1 and ISIS-2, and InterKosmos 19 (IK19), which have provided sets of topside data, but with a limited temporal and spatial coverage (Kutiev & Marinov, 2007; Kutiev et al., 2006; Nsumei et al., 2012; Wang et al., 2015b; Zhu et al., 2015). Others are based on RO measurements made by LEO satellites such as Challenging Minisatellite Payload and Constellation Observing System for Meteorology, Ionosphere, and Climate (COSMIC), now readily available with a good spatial and temporal global coverage (Olivares-Pulido et al., 2016; Stankov & Jakowski, 2006; Wang et al., 2015a; Wu et al., 2016; Xu et al., 2013). Effective scale heights were calculated also by using TEC data in conjunction with bottomside ionosonde-derived data to constrain the topside profile to meet some requirements on topside TEC values (Belehaki et al., 2012; Stankov et al., 2003). In situ electron density measurements collected by Langmuir probes onboard LEO satellites can also be used to model the topside profile constraining some analytical functions to pass through the electron density value measured by the satellite and that measured by an underlying ionosonde (Liu et al., 2014; Tulasi Ram et al., 2009; Venkatesh et al., 2011) or using electron density values measured by satellites flying at different heights (Třísková et al., 2006).

Liu, Le, et al. (2007) and Liu, Wan, et al. (2007), using Arecibo (66.7°W, 18.4°N) and Millstone Hill (71.5°W, 42.6°N) ISR measurements, made a careful morphological and theoretical examination of differences between H_p, H_m, and *VSH* (vertical scale height), where *VSH* is the effective scale height related to the topside part characterized by a constant value of the electron density gradient which is dominated by O^+ ions (Kutiev et al., 2006; Rishbeth & Garriott, 1969). From a theoretical point of view, Liu, Le, et al. (2007) and Liu, Wan, et al. (2007) pointed out that H_p and *VSH* would be equal only in a topside ionosphere mainly driven by a diffusive equilibrium and neglecting the altitude gradient of the thermospheric temperature, while *VSH* is expected to be twice H_m under diffusive equilibrium conditions. Analyzing Arecibo ISR data, they found that median ratios of *VSH* and H_p are about 0.9 by daytime and 1.3 at night, while median ratios of *VSH* and H_m are between 3.2 and 3.6 by daytime and equal to 2.8 at night. Similar results have been found also analyzing Millstone Hill ISR data. Liu, Le, et al. (2007) and Liu, Wan, et al. (2007) studies led to the important conclusions that (a) the dynamics of the topside ionosphere is dominated by the plasma diffusion and (b) motions caused

by the vertical thermal structure of this region, field-aligned fluxes, the ion-neutral drag, and neutral winds cannot, however, be neglected. Besides differences in the absolute values, plasma and effective scale heights exhibit different diurnal and seasonal behavior as well. Thus, there is a need to carefully specify that the scale height we are considering in this study is the effective scale height.

Fonda et al. (2005) compared α-Chapman, β-Chapman, Epstein, and modified Epstein (as used in the NeQuick topside model by Radicella and Leitinger, 2001, and Nava et al., 2008) profiles to those measured by ISIS-2 and IK19 topside sounders, finding that α-Chapman gives the best results. Moreover, they underlined the need to improve the topside formulation to better reproduce the experimental shape, especially for the higher part of the topside profile.

Verhulst and Stankov (2014, 2015) compared α-Chapman, β-Chapman, Epstein, and exponential topside profiles (calculating for each of these a different effective scale height) to topside sounders data, finding that in almost 75% of the analyzed cases the best fit was provided by the exponential profile, followed by the α-Chapman profile. Local time, seasonal, latitudinal, longitudinal, solar, and geomagnetic activity influence on the topside profile shape were also identified but highlighting at the same time an objective difficulty in modeling the effective scale height dependence on these parameters. More obvious relations were instead identified between the profile shape and the characteristics associated to the *F*2 layer peak (basically *hmF*2 and *NmF*2), whose variations strongly influence the topside profile. Verhulst and Stankov (2014, 2015) also stressed the fact that using a single profile for every geophysical condition and for the entire topside profile could lead to a misrepresentation, underlining that a two-layer profile composed by an α-Chapman function for the lower part of the topside region (from *hmF*2 to about 400 km of height) and an exponential function for the upper part (from 400 km to the upper transition height) could better describe the topside ionosphere.

Venkatesh et al. (2014) carried out a study to identify the altitude, above *hmF*2, at which to calculate the effective scale heights giving the most reliable representation of the topside profiles, when compared to those recorded by ISRs at Arecibo (66.7°W, 18.4°N) and Jicamarca (77.3°W, 11.9°S). To accomplish this task, they used an α-Chapman profile, joining the *F*2 layer peak point with that above with a constant effective scale height. After calculating effective scale heights for different local times and seasons, they found that H_m generally exhibits an increase with altitude for the first 50–100 km above the *F*2 layer peak height and then settles on a fairly constant value for the following 200–250 km. Comparing calculated α-Chapman topside vertical electron density profiles (using effective scale heights calculated between the *F*2 layer peak height and a varying point above) and ISR profiles, they got the best results for H_m values obtained using electron density values around 550 km for the Jicamarca equatorial station and around 500 km for the Arecibo low-latitude station.

The objective of this work is to provide an operational method to model the topside ionospheric vertical electron density profile. To this purpose, Swarm's Langmuir probe electron density data (Knudsen et al., 2017) and *F*2 layer peak characteristics provided by the International Reference Ionosphere UPdate (IRI UP) method (Pignalberi et al., 2018a, 2018b) are used in conjunction with several analytical functions dependent on an effective scale height parameter. Effective scale heights are calculated by forcing the passage of the considered analytical functions through two anchor points (one at the height *hmF*2 of the *F*2 layer peak and the other one at the height h_{sat} of the satellite) and then modeled as a function of the *F*2 layer critical frequency *foF*2 and *hmF*2. The result of this study is then a tool, namely, grids of H_m as a function of *foF*2 and *hmF*2, to reliably model the topside over the European region, once *foF*2 and *hmF*2 are known, either measured or modeled.

Section 2 describes how satellites' measured electron density values and *F*2 layer peak characteristics have been used to calculate effective scale heights using several topside analytical functions. Section 3 describes the method by which the calculated effective scale heights have been modeled in order to be suitable from an operational point of view. In the same section a validation of the proposed method is also shown. Conclusions are the subject of section 4.

2. Data and Method

By assuming a constant effective scale height H_m for the first hundreds of kilometers from the *F*2 layer peak, one can model the topside above some selected ionosonde stations using an analytical formula joining the

*F*2 layer peak characteristics *NmF*2 and *hmF*2, measured by the ionosonde, to the in situ electron density value $N(h_{sat})$ measured by the satellite at the altitude h_{sat}; for this study satellites of the Swarm mission are considered.

Tulasi Ram et al. (2009) and Venkatesh et al. (2011) pursued this approach using simultaneous observations of Republic Of China SATellite-1 (ROCSAT-1) electron density values (collected around 600 km of altitude) and ionosonde or ISR-deduced *F*2 layer characteristics. However, selecting only satellite's passages on a definite point (the one where a ground-based measuring station is installed) heavily reduces the available data and consequently the possibility to do any spatial study on the topside effective scale height. Furthermore, ionosondes (or ISRs) positioning and the corresponding sounding repetition rate further reduce available data, thus limiting the spatial and temporal description of any modeled parameter. To overcome this limitation, Liu et al. (2014) modeled the ROCSAT-1 electron density measurements as a function of local time, season, longitude, and solar activity; then, they extrapolated the electron density behavior at ROCSAT-1 height for the Wuhan location (30.6°N, 114.4°E), where an ionosonde is installed. In this way, using the Tulasi Ram et al. (2009) and Venkatesh et al. (2011) approach, they were able to obtain a large effective scale height statistics over Wuhan as a function of local time, and day of the year, for two selected solar activity levels.

An ionospheric model able to spatially describe the ionospheric plasma, more specifically the *F*2 layer characteristics, would maximize the use of the data recorded by the Swarm constellation. This task can be accomplished for the European region by the IRI UP method recently proposed by Pignalberi et al. (2018a, 2018b), which can generate European maps (from 15°E to 45°W in longitude and from 30°N to 60°N in latitude) of updated values of *foF*2 and *hmF*2. In this way, the effective scale height can be calculated for each satellite's passage over Europe, averaging the satellite's measurements falling in each grid point of the map, which is considered in this work with a $1° \times 1°$ spatial resolution. This procedure allows us to take advantage of every satellite's track over the European region and not of only the ones right over a ground-based station. Carrying out this analysis for every transit of each satellite of the Swarm constellation over each grid point of the European region, a huge amount of effective scale height values can be obtained. This gives the possibility to perform a robust statistical and spatial characterization of this parameter.

2.1. Swarm's Satellites Constellation Data

Swarm is a satellite constellation launched at the end of 2013 by the European Space Agency (Friis-Christensen et al., 2006). It is constituted by three LEO satellites in a circular near-polar orbit. Two of them (called Alpha (A) and Charlie (C)) are orbiting the Earth side by side at the same altitude of about 460 km (with an inclination of 87.4°, an east-west separation of 1–1.5° in longitude and a maximal differential delay in orbit of approximately 10 s), while the third (Bravo (B)) is flying about 60 km above (with an inclination of 88°) in an orbital plane which will gradually get farther from those of the other two satellites during the mission's lifetime (9 h in local time after 4 years).

They are all equipped with identical instruments consisting of high-resolution sensors for measurements of both geomagnetic and electric fields, as well as plasma density. In particular, we are interested mainly in the electron density measurements at 2 Hz rate made by the Langmuir probes carried by each satellite.

We used the "Extended Set of Swarm Langmuir Probe Data" data set (SW-RN-IRF-GS-005, Rev: 1, 2016-06-23), released by S. Buchert (Swedish Institute of Space Physics) on 23 June 2016 (freely downloadable at https://earth.esa.int/web/guest/swarm/data-access after registration). This data set comprises calibrated plasma density measurements collected by the Swarm satellite constellation from 12 December 2013 to 11 June 2016. Specifically, Swarm's measurements collected over the European region (from 15°W to 45°E in longitude and from 30°N to 60°N in latitude) have been considered. In particular, we used 4,259,984; 4,229,607; and 4,251,095 electron density measurements for Swarm A, B, and C, respectively. From this data set, unusable data have been eliminated according to a flag embedded in the downloaded files, as recommended in the Extended Set of Swarm Langmuir Probe Data data set (SW-RN-IRF-GS-005, Rev: 1, 2016-06-23).

The near-polar orbit of satellites, the particular geometry of the constellation, and the height at which satellites fly are particularly appropriate to study the topside ionosphere. As it is evident from Figure 1, Swarm satellites provide a good spatial (both in longitude and latitude) and temporal (local time and seasonal) coverage of the European region.

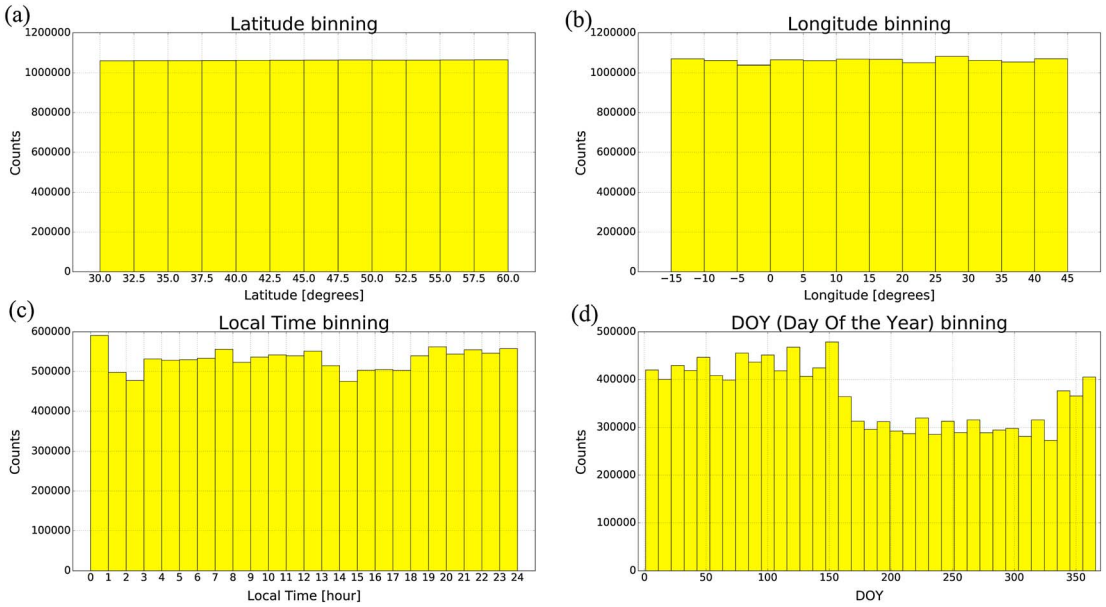

Figure 1. Swarm satellites' data distribution over the European region from 12 December 2013 to 11 June 2016 in terms of (a) latitude, (b) longitude, (c) local time, and (d) DOY (day of the year).

2.2. IRI UP *foF2* and *hmF2* Maps Generation

The IRI UP method (Pignalberi et al., 2018a, 2018b) has the purpose to update the IRI model through the assimilation of the *foF*2 and *M*(3000)*F*2 ionospheric characteristics recorded routinely by a network of European ionosondes. Such measurements are used to calculate at each ionosonde location the effective values IG_{12eff} and R_{12eff} of indices IG_{12} (the 12 months running mean of the ionospheric activity index *IG*; R. Y. Liu et al., 1983) and R_{12} (the 12 months running mean of the Zurich sunspot number *R*) that are then used to generate two-dimensional European maps of these indices through the application of the Universal Kriging method (Kitanidis, 1997). The computed maps are then used as input for the IRI model (the IRI 2016 version was used throughout the analysis in this paper) to synthesize updated values of *foF*2 and *hmF*2 over the European region. Since in the IRI model the *F*2 layer is an anchor point for the electron density vertical profile, updating *foF*2 and *hmF*2 characteristics (through IG_{12eff} and R_{12eff} effective indices) automatically changes the whole profile.

Values of *foF*2 and *M*(3000)*F*2, recorded at minutes 00 and 30 of each hour by the European stations listed in Table 1, have been assimilated by IRI UP. This means that, at minutes 00 and 30 of each hour, maps of updated values of *foF*2 and *hmF*2 are produced by the IRI UP method. In this way, the time difference between the satellite's passage and the updated maps of *foF*2 and *hmF*2 is 15 min at most (because if the satellite passage is, for instance, at 12:37, IRI UP maps considered will be the ones at 12:30, with a corresponding time difference equal to 7 min; instead, if the satellite passage is at 12:46, we do not have to consider IRI UP maps recorded at 12:30 but the ones recorded at 13:00, and so the time difference becomes 14 min, in any case always lower than or at maximum equal to 15 min). Ionosonde data were downloaded from the Digital Ionogram DataBASE (Reinisch & Galkin, 2011) by means of the Standard Archival Output (SAO) Explorer software developed by the University of Massachusetts, Lowell. It is worth noting that values recorded at the stations listed in Table 1 were autoscaled by different algorithms: Automatic Real-Time Ionogram Scaler with True height (ARTIST, Galkin & Reinisch, 2008; Reinisch & Huang, 1983) and Autoscala (Pezzopane et al., 2010; Pezzopane & Scotto, 2010). Concerning *foF*2 and *M*(3000)*F*2, the ionospheric characteristics of the *F*2 region we are interested in for this study, Autoscala proved to be more reliable than ARTIST (Pezzopane & Scotto, 2005, 2007), and in the last years this reliability has been increased thanks to several filters that have been added to the image processing technique used by Autoscala (Pezzopane & Scotto, 2010; Scotto & Pezzopane, 2008a, 2008b). Anyway, before doing the analysis described in this paper, and in order to have a data set of *foF*2 and *M*(3000)*F*2 values as much reliable as possible, each ionogram has been visually validated and the corresponding output corrected when necessary.

Table 1
European Ionosonde Stations for Which foF2 and M(3000)F2 Values Have Been Assimilated by the IRI UP Method (Slightly Modified From Pignalberi et al., 2018a)

Ionospheric stations	Longitude (deg)	Latitude (deg)	Ionosonde type	Autoscaling software
Athens	23.5°E	38.0°N	Digisonde DPS-4D	ARTIST 5
Chilton	0.6°W	51.5°N	Digisonde DPS-1	ARTIST 4
Dourbes	4.6°E	50.1°N	Digisonde DPS-4D	ARTIST 5
El Arenosillo	6.7°W	37.1°N	Digisonde DPS-4D	ARTIST 5
Gibilmanna	14.0°E	37.9°N	AIS-INGV	Autoscala 4.1
Fairford	1.5°W	51.7°N	Digisonde DPS-4D	ARTIST 5
Juliusruh	13.4°E	54.6°N	Digisonde DPS-4D	ARTIST 5
Moscow	37.3°E	55.5°N	Digisonde DPS-4	ARTIST 5
Nicosia	33.2°E	35.0°N	Digisonde DPS-4D	ARTIST 5
Pruhonice	14.6°E	50.0°N	Digisonde DPS-4D	ARTIST 5
Rome	12.5°E	41.8°N	AIS-INGV	Autoscala 4.1
Roquetes	0.5°E	40.8°N	Digisonde DPS-4D	ARTIST 5
San Vito	17.8°E	40.6°N	Digisonde DPS-4D	ARTIST 5
Warsaw	21.1°E	52.2°N	VISRC2	Autoscala 4.1

Note. IRI UP = International Reference Ionosphere; DPS = Digisonde Portable Sounder; AIS-INGV = Advanced Ionospheric Sounder-Istituto Nazionale di Geofisica e Vulcanologia; VISRC2 = Ionosonde developed by the Polish Space Research Center; ARTIST = Automatic Real-Time Ionogram Scaler with True height.

2.3. Topside Analytical Formulation

Four different analytical functions are used to model the topside ionospheric electron density profile, as a function of both the effective scale height (H_m) and the *F*2 layer peak characteristics (*NmF*2 and *hmF*2). These are as follows:

1. α-Chapman:

$$N(h) = NmF2 \cdot \exp\left\{\frac{1}{2}\left[1 - \frac{h - hmF2}{H_m} - \exp\left(-\frac{h - hmF2}{H_m}\right)\right]\right\}, \tag{1a}$$

2. β-Chapman:

$$N(h) = NmF2 \cdot \exp\left\{\left[1 - \frac{h - hmF2}{H_m} - \exp\left(-\frac{h - hmF2}{H_m}\right)\right]\right\}, \tag{1b}$$

3. Epstein:

$$N(h) = 4 \cdot NmF2 \frac{\exp\left(\frac{h-hmF2}{H_m}\right)}{\left[1 + \exp\left(\frac{h-hmF2}{H_m}\right)\right]^2}, \tag{1c}$$

4. Exponential:

$$N(h) = NmF2 \cdot \exp\left(-\frac{h - hmF2}{H_m}\right). \tag{1d}$$

The different empirical methods listed in section 1 make use of one or more of the aforementioned analytical topside functions. Among these, the most used and studied is the α-Chapman with a fixed (Chapman, 1931; Wright, 1960) or variable (Vary-Chap) effective scale height (Reinisch et al., 2007; Rishbeth & Garriott, 1969). The use of Chapman's functions to model the topside ionosphere was carefully investigated by Luan et al. (2006) studying which Chapman's shape factor (keeping constant the effective scale height) could better fit ISR-derived profiles at Arecibo (18.4°N, 66.7°W) and Millstone Hill (42.6°N, 71.5°W). They found that a value of the Chapman shape factor of about 0.5 (as it is in the α-Chapman function) gives a reasonable description of the topside ionosphere, but with some departures in the morning (where values of about 0.35–0.45 were identified) and during daytime (where values of about 0.55–0.75 were identified), showing also a seasonal variation. The Chapman's shape factor exhibits a high correlation with the *F*2 layer peak electron density and shows a strong solar cycle dependence during the late morning hours. Zhang et al. (2002) tried to model the topside ionosphere by fitting the α-Chapman and Epstein functions, with a linearly variable effective scale height, to ISR profiles collected in Malvern (52.1°N, 2.3°W). They found that topside profiles can be fitted very well (about 94% of profiles met the criterion $\varepsilon < 10\%$, ε being the percentage difference between modeled

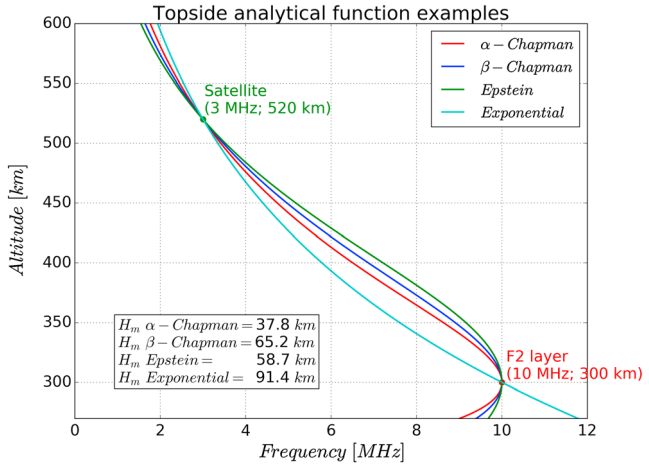

Figure 2. Examples of topside analytical functions (1a)–(1d) obtained after forcing them to meet the constrain to join the *F*2 layer peak point (red dot) to the satellite point (green dot). Corresponding calculated effective scale heights are all different.

and measured topside electron density values) to a height of about 400 km above the *F*2 peak using either functions.

Despite being widely used, Chapman's functions are not based on any theoretical consideration, because they were derived according to the simplifying hypotheses of monochromatic solar irradiance, single ion component, and, more importantly, absence of any dynamics (Chapman, 1931). Such hypotheses do not hold in the *F*2 region, where the dynamics of the ions is deeply influenced by both zonal and meridional neutral winds and the effect of the diffusion along the geomagnetic field lines, and do not hold even more so in the topside ionosphere. For these reasons, other analytical functions were used to model the topside ionosphere. Among these, Epstein and exponential functions meet the constraint to pass through the *F*2 layer peak and to monotonically decrease in the topside ionosphere. All the analytical functions (1a)–(1d) are purely empirical, thus the need to find which of these can better describe the topside ionosphere.

An example of the four selected topside profiles is displayed in Figure 2; it is worth noting that despite having the same two anchor points (one at the height of the *F*2 layer peak and the other one at the height of the satellite), they are different, especially in the region right above the *F*2 layer peak, which is the one we focus on. This means that the calculated effective scale heights are different. Most of the work is then devoted to the search of the function able to better represent the shape of the topside. With regard to this, Chapman and Epstein functions were introduced to better describe the shape of the *F*2 layer. The exponential one, which is not able to describe the characteristic curvature of this layer, has instead the potential to better describe the upper part of the topside, where the ionosphere transitions to the plasmasphere (in which the vertical profile is essentially exponential with a scale height dependent on the H^+ions vertical distribution). In light of these considerations, the choice of which function has to be used to model the topside ionosphere is not trivial and deserves a close inspection.

2.4. COSMIC/FORMOSAT-3 Radio Occultation Data

COSMIC, also known as FORMOSAT-3 in Taiwan, is a constellation made by six microsatellites launched on 15 April 2006 into a circular orbit (with 72° of inclination) at about 800 km of height (gradually reached 17 months after the launch) and a separation angle of 30° in longitude between neighboring satellites (Anthes et al., 2008). The mission is a collaborative project between the National SPace Organization in Taiwan and the University Corporation for Atmospheric Research in the United States. Each satellite carries a Global Positioning System radio occultation receiver able to measure the phase delay of radio waves from Global Positioning System satellites as they are occulted by the Earth's atmosphere, allowing an accurate determination of the ionospheric vertical electron density profile. It is worth noting that the accuracy and the precision of the RO data critically depend on the algorithm used in the inversion procedure to obtain a vertical electron density profile. In particular, COSMIC RO profiles are obtained by means of the Abel inversion technique (Haji & Romans, 1998; Schreiner et al., 1999). Because of the assumed spherical symmetry in the Abel inversion procedure, some errors arise above all in the equatorial ionization anomaly region, during dawn and dusk hours and during intense magnetically disturbed events (Garcia-Fernandez et al., 2003; Yue et al., 2010). This is due to the strong horizontal electron density gradients characterizing these ionospheric states, a condition that the spherical symmetry assumption, embedded in the Abel inversion technique, cannot take into account.

Comparing COSMIC retrieved *NmF*2 and *hmF*2 characteristics with those measured by co-located midlatitude ionosondes in the European region for the year 2008, Krankowski et al. (2011) found a good agreement in terms of both absolute value and degree of correlation, thus highlighting the good reliability of COSMIC data over the European region.

RO derived electron density profiles collected by COSMIC satellites, for the same period covered by Swarm's data (from 12 December 2013 to 11 June 2016) and whose tangent points of signal ray path were over the

considered European region (from 15°W to 45°E in longitude and from 30°N to 60°N in latitude), have been used to validate our method and to decide which of the four proposed topside analytical formulations performs better. The data set consists of 17,872 "ionprf" RO profiles, downloaded from the COSMIC Data Analysis and Archive Center (http://cdaac-www.cosmic.ucar.edu/cdaac/products.html).

RO profiles showing *foF*2 and *hmF*2 values outside the range [1,16] MHz and [150, 450] km, respectively, were discarded, as well as profiles with excessive and unrealistic fluctuations in the electron density. We remind here that *foF*2 is directly related to *NmF*2 by means of the relation

$$foF2\ (\mathrm{MHz}) = \sqrt{NmF2\ (\mathrm{el/cm^{-3}})/\left(1.24{\cdot}10^4\right)}. \tag{2}$$

After applying this filtering procedure, the remaining profiles were 9,672 (about 54% of the total).

In this work, COSMIC RO data have been used as truth reference because of their reliability in the description of the topside ionosphere and the underlying *F* region (Chu et al., 2010; Habarulema et al., 2014; Krankowski et al., 2011; Lei et al., 2007; Wu et al., 2009; Yue et al., 2010).

3. Effective Scale Height Modeling and Statistical Assessment

3.1. Effective Scale Height Modeling

Effective scale height values, calculated using the procedure described in section 2, need to be modeled as a function of some measured or modeled parameters. Many attempts were made in the past to model effective scale height values as a function of spatial (geocentric or magnetic longitude and latitude), temporal (local time, day of the year, and season), and solar and magnetic activity parameters. All these approaches led to different results, critically depending on the chosen modeling parameters and on the chosen modeling methods. Verhulst and Stankov (2014), studying which of the topside profile expressions (1a)–(1d) could better match Alouette and ISIS topside sounder profiles, using the Kutiev and Marinov (2007) topside scale height calculation method, came to the following conclusion.

1. Local time, season, magnetic longitude/latitude, solar activity, and geomagnetic activity have a crucial influence on the topside profile shape. However, they say, "commonly used solar/magnetic activity indices do not provide much useful information and criteria to select a particular topside profile. The same holds true for local time, season, and magnetic latitude/longitude".
2. Difficulties in modeling the effective scale height as a function of commonly used indices or geophysical parameters arise from the simultaneous influence that these drivers have on the topside ionosphere. Thus, it is difficult to discriminate the influence of each driver.
3. More obvious relations exist between the topside profile shape and the *F*2 layer peak characteristics, especially between *hmF*2 and the effective scale height.

At this point of the analysis, the effective scale height H_m, calculated in section 2, is a function of four variables:

$$H_m = H_m(hmF2, NmF2, h_{sat}, N(h_{sat})). \tag{3}$$

From an operational point of view it would be better to describe H_m as a function of only *Nm*F2 and *hmF*2, which are measured by ionosondes or easily modeled by several ionospheric models, while satellite's related parameters are not routinely available. Therefore, according to Verhulst and Stankov (2014), H_m values are modeled as a function of *hmF*2 and *foF*2, with a bin width of 5 km and 0.25 MHz, respectively. We want to stress here the fact that using *foF*2, instead of *NmF*2, is done only for convenience. In this way any dependence on h_{sat} and $N(h_{sat})$ is neglected:

$$H_m = H_m(hmF2, foF2). \tag{4}$$

For each of the four proposed topside profiles and for each Swarm's satellite-derived data set, a two-dimensional binning procedure was then carried out, by selecting calculated H_m values derived from a defined pair (*foF*2, *hmF*2) of binning indices. In order to obtain a two-dimensional map of H_m, function of *foF*2 and *hmF*2, the median of the H_m values falling in each bin was calculated.

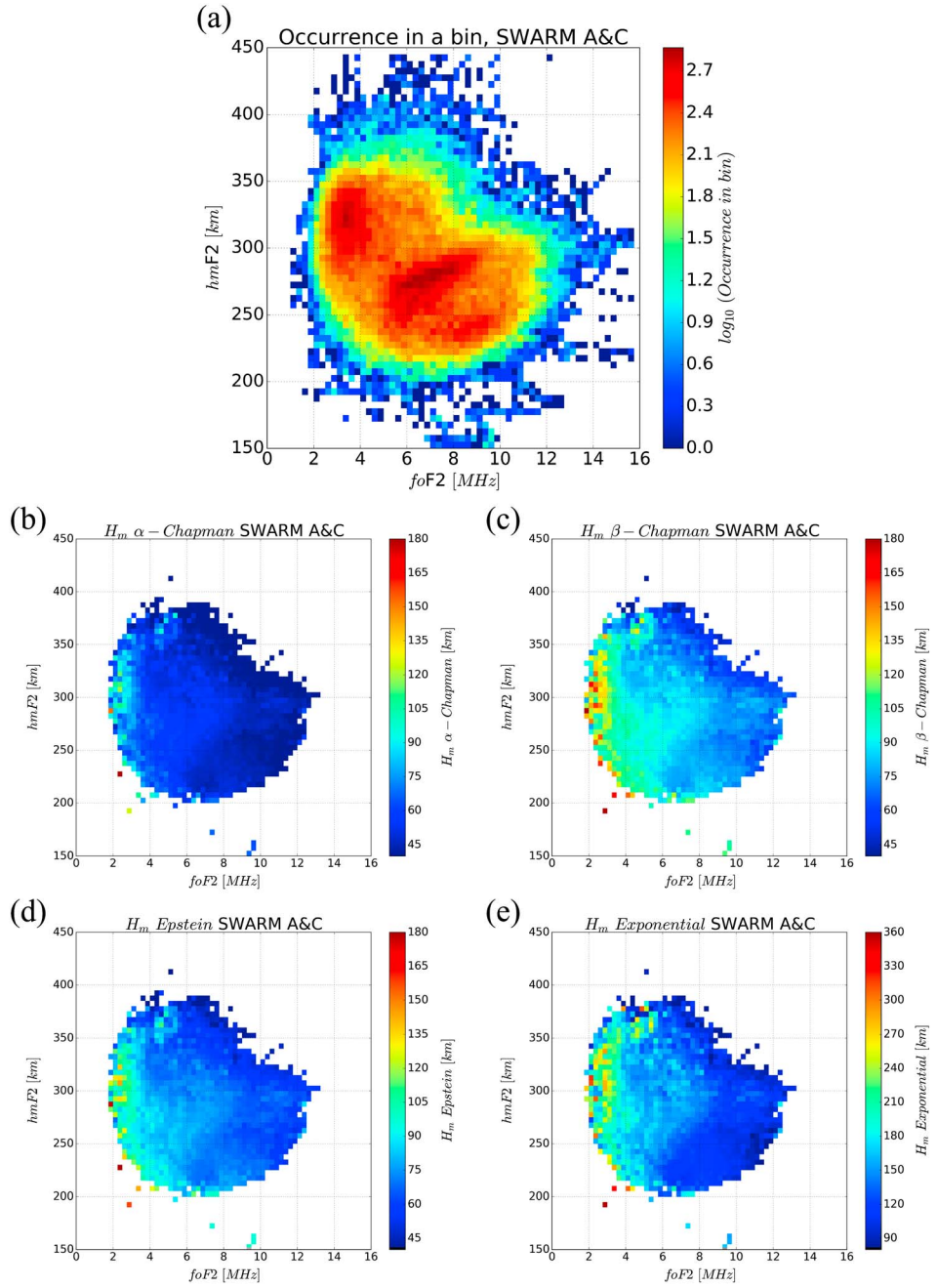

Figure 3. (a) Effective scale height values occurrence in a bin (logarithmic scale). Median values of the effective scale height are shown for (b) the α-Chapman topside profile, (c) the β-Chapman topside profile, (d) the Epstein topside profile, and (e) the exponential topside profile. It is worth noting that the scale of the exponential effective scale height is doubled. For each plot the joint data set Swarm A and C was considered. In panels (b)–(e), bins including a number of H_m values lower than 10 (the blue/dark blue ones in panel (a)) have been discarded.

Figure 3 shows the calculated H_m two-dimensional binning grids, after joining Swarm A and C data sets (the choice to join Swarm A and C data sets will be justified later), using each of the (1a)–(1d) topside profiles. The distribution of the number of values falling in each bin is shown in Figure 3a; for statistical robustness, a value of H_m was calculated only when this number was greater than 10. The minimum number of values in a bin is 0, represented by the white color, while the maximum number of values in a bin is 735, corresponding to the dark red color. Overall, there are 204,086 values to be binned in 60 × 64 = 3,840 bins. If the values were

uniformly distributed, there would be about 53 values in each bin; anyhow, because this is not the case (only about 2,000 bins are filled), we decided to set a threshold that is a 10th of the number of values in a bin that there would be if the values were uniformly distributed in each filled bin (≈200,000 values/2,000 bins/10 = 10). Figure 3a shows that binning indices ranges are *foF*2 ∈ [0, 16] MHz and *hmF*2 ∈ [150, 450] km and that the most filled bins (the orange/red colored ones) are in the range [2, 11] MHz for *foF*2 and [225, 350] km for *hmF*2. Obviously, these are the bins for which the highest confidence level, in a statistical sense, is achieved. Figure 3a also shows the presence of two well-distinguished patterns highlighted by the dark red sectors, one in the sector between 2 and 4 MHz for *foF*2 and between 300 and 350 km for *hmF*2 and the other one in the sector between 5 and 9 MHz for *foF*2 and between 250 and 300 km for *hmF*2. These two patterns describe, approximately, the nighttime and daytime behaviors of the pair (*foF*2, *hmF*2), respectively. This means that, for most of local time hours, daytime and nighttime behaviors do not overlap with each other, allowing a reliable description of the corresponding topside ionosphere.

Figures 3b–3e depict the two-dimensional binning grids of the effective scale height median values for each of the considered topside analytical functions. The bin distribution reflects what is shown in Figure 3a, but bins with a number of H_m values lower than 10 are not displayed. For each topside profile, the highest H_m median values are obtained for low *foF*2 values, and then they decrease for higher *foF*2 values. Extremely high H_m median values, obtained mainly for very low *foF*2 values (dark red bins), could be due to an unsatisfactory statistical description in those bins. Generally speaking, α-Chapman-derived H_m median values are characterized by the lowest values. β-Chapman and Epstein calculated H_m median values are slightly higher than α-Chapman ones. Note that the scale for the exponential H_m median values is double compared to those of the other three functions. As explained in section 2, this significant difference between the exponential profile and the other ones can be ascribed to the very different behavior of the exponential profile immediately above the *F*2 layer peak.

Once grids of the median effective scale height as a function of *foF*2 and *hmF*2 are obtained (like those shown in Figure 3), one can use them to model the topside profile. In fact, once a pair of values (*foF*2, *hmF*2) is available, either measured or modeled, a value of the corresponding effective scale height can be extrapolated from the map of each topside function.

In addition to the grids of effective scale height median values, grids of effective scale height first and third quartile values have been also calculated (not shown here), in order to characterize the variability of this parameter and to provide an estimation of the error associated to a defined effective scale height value. In this way, topside vertical electron density profiles derived using effective scale height median values can be complemented with lower and upper profiles calculated by using effective scale height first and third quartile values.

3.2. Effective Scale Height Dependence on the Satellite Altitude

Neglecting the dependence of the effective scale height on satellite's parameters (h_{sat}, $N(h_{sat})$), as described in section 3.1, implies an approximation; this is because we are trying to describe a four-dimensional mathematical function while utilizing only two of its four independent variables. Since the three Swarm's satellites fly at different heights (around 460 km for Swarm A and C and around 520 km for Swarm B), a careful analysis of the effective scale heights calculated using electron density data derived from different satellites has to be carried out. For this reason, effective scale height median values have been calculated using, separately, each of the measurement data sets provided by Swarm's satellites, and differences, bin by bin, have been calculated for all the possible permutations.

An example of this analysis is visible in Figure 4, for the α-Chapman topside profile. This figure shows that, except for some bins in sectors statistically not so significant, differences between Swarm A and C are negligible. This led us to merge Swarm A and C data sets to derive the effective scale heights shown in Figure 3. The same does not hold true for Swarm B-derived effective scale heights, which are different from those derived from Swarm A and C. Differences of the order of about 10–20 km, for *foF*2 values lower than 6 MHz, and of about 0–10 km, for *foF*2 values higher than 6 MHz, are appreciable. Thus, effective scale height values derived from Swarm B cannot be merged with those calculated by using Swarm A and C.

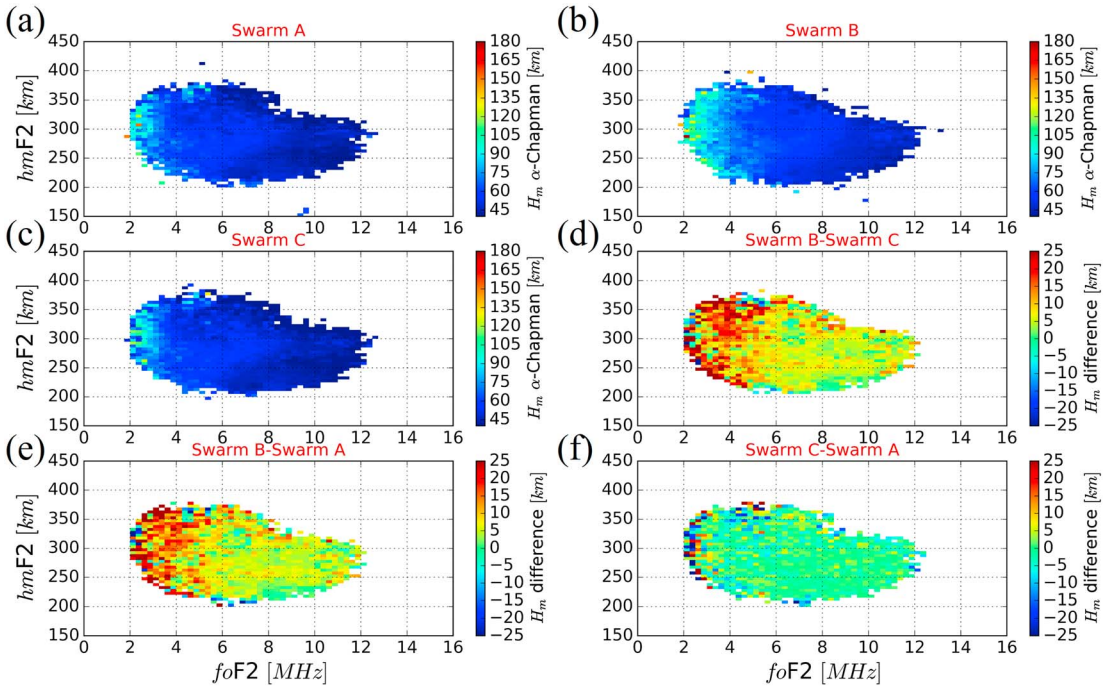

Figure 4. Median effective scale height values for the α-Chapman topside profile, for (a) the Swarm A data set, (b) the Swarm B data set, and (c) the Swarm C data set. Corresponding differences are shown in panels (d), (e), and (f).

Results shown in Figure 4 seem to contradict the work hypothesis behind the whole carried out analysis, namely, the constancy of the topside effective scale height for the ionospheric region we are focused on. In reality, this should not be a surprise because it is only a consequence that the dependence of the effective scale height on satellite's parameters has been deliberately neglected.

The work hypothesis can be verified by using normalized variables in the description of the effective scale height, that is,

$$n = \frac{N(h)}{NmF2}, z = h - hmF2. \tag{5}$$

Using (5), the topside analytical formulas become

1. Normalized α-Chapman:

$$n(z) = \exp\left\{\frac{1}{2}\left[1 - \frac{z}{H_m} - \exp\left(-\frac{z}{H_m}\right)\right]\right\}, \tag{6a}$$

2. Normalized β-Chapman:

$$n(z) = \exp\left\{\left[1 - \frac{z}{H_m} - \exp\left(-\frac{z}{H_m}\right)\right]\right\}, \tag{6b}$$

3. Normalized Epstein:

$$n(z) = 4\,\frac{\exp\left(\frac{z}{H_m}\right)}{\left[1 + \exp\left(\frac{z}{H_m}\right)\right]^2}, \tag{6c}$$

4. Normalized Exponential:

$$n(z) = \exp\left(-\frac{z}{H_m}\right). \tag{6d}$$

In this way, calculated effective scale heights depend only on the two normalized variables:

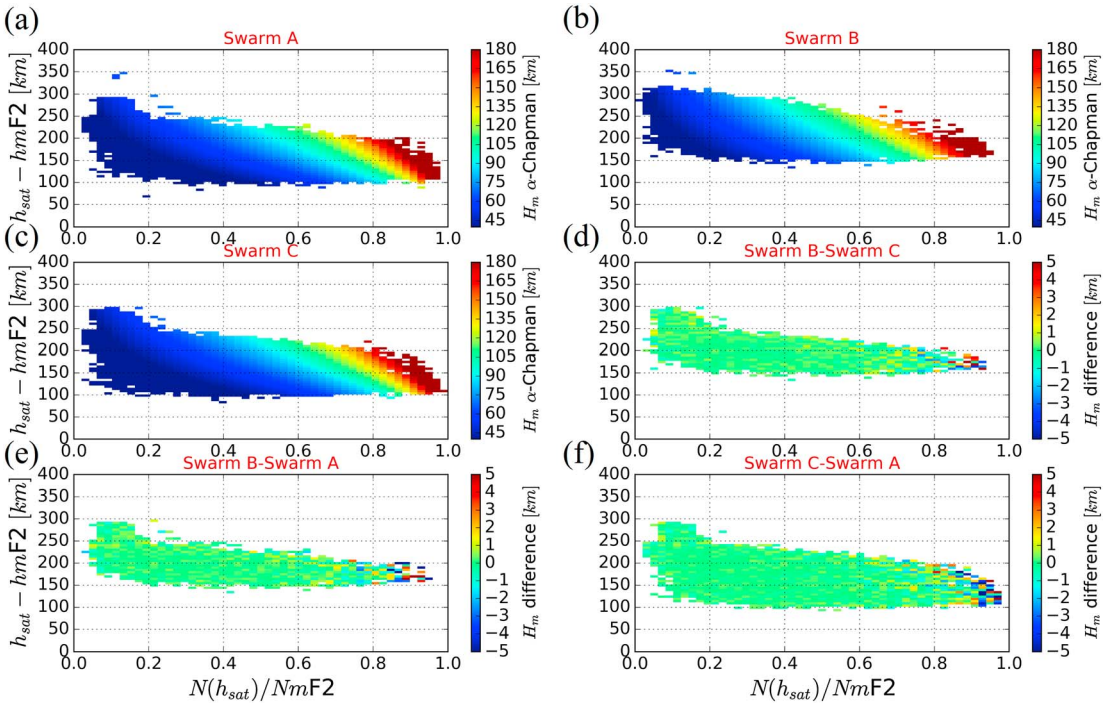

Figure 5. Same as Figure 4 but using normalized variables. Compared to Figure 4, the scale of the last three panels is reduced by one fifth.

$$H_m = H_m(n, z). \tag{7}$$

Using (7) to make exactly the same calculations done to obtain Figure 4, we obtain the results shown in Figure 5.

This figure shows that independently of which Swarm satellites are used, the difference between effective scale height median values is close to zero (the scale of the last three panels in Figure 5 is reduced by one fifth compared to Figure 4), which confirms the validity of the effective scale height constancy hypothesis, for the studied ionospheric region.

The use of normalized variables, even though it looks attractive, is not feasible from an operational point of view because of the lack of available real-time electron density values recorded by LEO satellites. Thus, there is a need to use the approach described in section 3.1, relying on only the *F*2 layer peak characteristics, separating the data set formed by Swarm A and C data from the one related to Swarm B.

3.3. Topside Analytical Formulation Statistical Assessment

Following the procedure described in section 3.1, we calculated two-dimensional binning grids of the median effective scale height for each of the four proposed topside profile and for each of the two satellite's derived data sets related to Swarm A and C and Swarm B, respectively. The number of calculated binned grids is then eight.

To investigate the performance of the proposed method in modeling the lower ionospheric topside profile and to assess which of the four proposed topside profiles better represents this region, a careful statistical analysis has been carried out using an independent data set of topside profiles. Specifically, RO-derived electron density profiles collected by COSMIC/FORMOSAT-3 (as described in section 2.4) have been used as truth reference.

For each of the considered 9,672 COSMIC profiles, the root mean square error (RMSE, equation (8)) and the normalized root mean square error (NRMSE, equation (9)), between modeled topside electron density values and those measured by COSMIC (both expressed as plasma frequency, f_p, obtained replacing *NmF*2 with the electron density N_e in equation (2)), have been calculated for the height range from *hmF*2 to the height of Swarm's satellites:

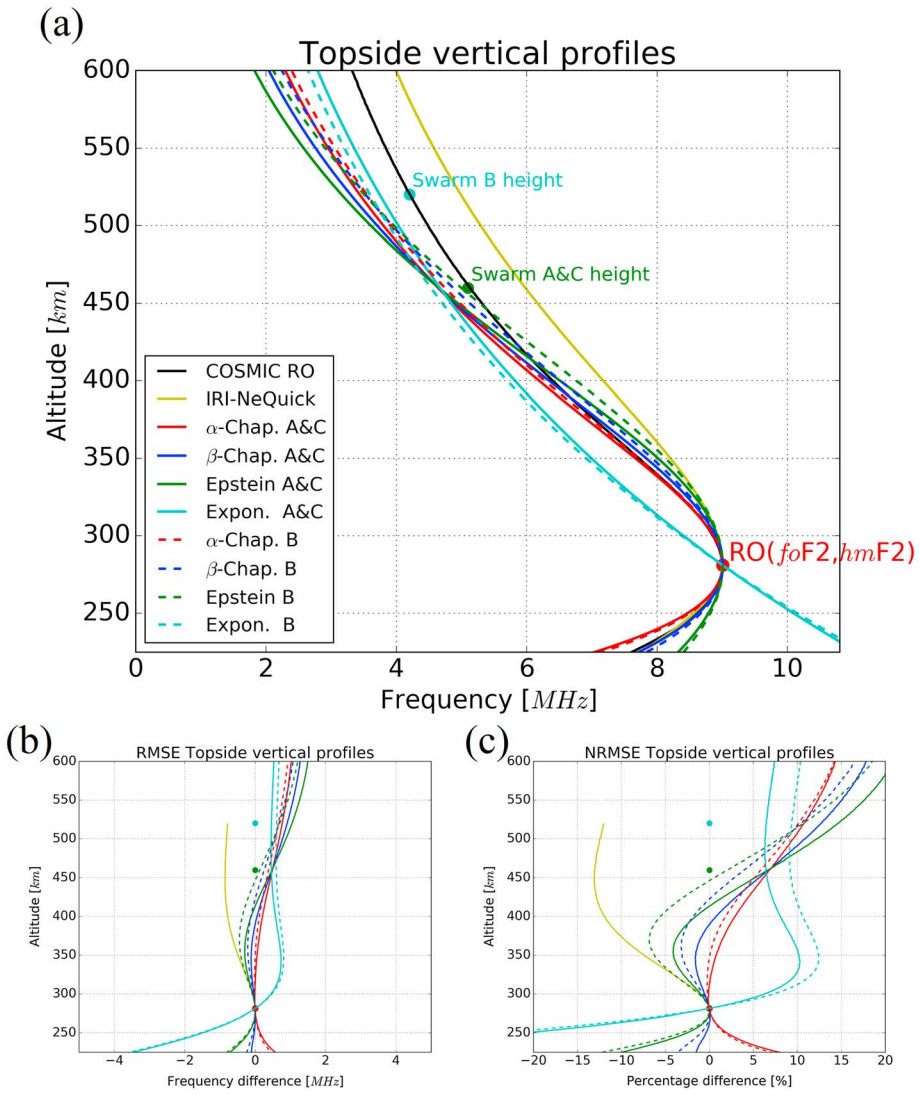

Figure 6. (a) Topside electron density profile derived from the Constellation Observing System for Meteorology, Ionosphere, and Climate Radio Occultation (COSMIC RO) measurement (black solid line), and those modeled by our method using the Swarm A and C data set (red, blue, green, and light blue solid lines) and using the Swarm B data set (red, blue, green, and light blue dashed lines). The dark yellow solid line depicts the topside profile as modeled by the International Reference Ionosphere (IRI) model (using the NeQuick topside option), after forcing the model to pass through the measured RO-derived *F*2 layer peak point. (b) root mean square error (RMSE) values. (c) normalized root mean square error (NRMSE) values.

$$\mathrm{RMSE}\ [\mathrm{MHz}] = \sqrt{\frac{\sum_{i=1}^{N}\left(f_{\mathrm{p_{model},i}} - f_{\mathrm{p_{COSMIC},i}}\right)^2}{N}}, \tag{8}$$

$$\mathrm{NRMSE}\ [\%] = \frac{\mathrm{RMSE}}{\overline{f_{\mathrm{p_{COSMIC}}}}} \cdot 100. \tag{9}$$

Modeled topside profiles have been calculated using the four profiles (1a)–(1d) and considering (a) *hmF*2 and *foF*2 values measured by COSMIC and (b) the effective scale height value, correspondent to values in (a), given by the two-dimensional binning map (as those shown in Figure 3) related to the definite topside profile. An example of the carried out analysis, for one of the analyzed COSMIC RO profiles, is shown in Figure 6.

The use of RO topside profiles leads, unavoidably, to some approximations because, actually, these are slanted than vertical. *hmF*2 and *foF*2 values derived by the RO method have a different spatial location compared to the other points of the profile, while the effective scale height calculated with our method refers to

Table 2
Statistical Summary of the Analysis Made by Comparing Modeled Topside Profiles With Those Measured by COSMIC Satellites

	Swarm A and C					Swarm B				
	α-Chapman	β-Chapman	Epstein	Exponential	IRI-NeQuick	α-Chapman	β-Chapman	Epstein	Exponential	IRI-NeQuick
	RMSE (MHz) data set (2014/121 to 2016/163)									
Mean	0.30	0.31	0.33	0.42	0.34	0.34	0.38	0.44	0.37	0.37
Standard deviation	0.22	0.22	0.23	0.31	0.35	0.20	0.22	0.25	0.23	0.34
	NRMSE (%) data set (2014/121 to 2016/163)									
Mean	6.14	6.44	7.14	7.94	7.00	8.69	9.59	11.04	8.39	8.31
Standard deviation	4.32	4.57	5.07	4.08	6.67	6.29	6.57	7.10	4.31	7.12

Note. COSMIC = Constellation Observing System for Meteorology, Ionosphere, and Climate; IRI = International Reference Ionosphere; RMSE = root mean square error; NRMSE = normalized root mean square error.

the whole topside vertical electron density profile. To get an idea of the co-location errors affecting this comparison, we have calculated, for each of the considered 9,672 RO profiles, the geographical difference, in degrees, between the *F*2 layer peak and the topside point at 460 km (the height of Swarm A and C) and 520 km (the height of Swarm B). The corresponding mean and standard deviation are as follows:

1. Mean co-location error, Swarm A and C = 2.4°
2. Mean co-location error, Swarm B = 3.3°
3. Standard deviation co-location error, Swarm A and C = 1.6°
4. Standard deviation co-location error, Swarm B = 2.2°

The mean co-location error is of the order of 2°–3°, with a dispersion of about 2°. Because of the known correlation distance of the ionosphere at midlatitudes, which is 1,000–1,500 km for quiet geomagnetic conditions (Klobuchar & Kunches, 2000; Yue et al., 2007), we think that this co-location error is not so important as to invalidate the analysis. Anyhow, a reduced performance of the proposed method can be expected when comparing it to RO-derived profiles.

A statistical summary of the analysis is shown in Table 2, where the mean and the standard deviation of both RMSE and NRMSE of all the 9,672 analyzed topside profiles are reported for each of the four studied topside profiles and also for the NeQuick topside option of the IRI model (Coisson et al., 2006), for both considered Swarm data sets. The NeQuick topside option of IRI has been chosen because, when compared to the other two possible options proposed by IRI, it turns out to be the best one (Bilitza, 2009). Moreover, as it has been shown recently by Pignalberi et al. (2016), the IRI topside description performs better for midlatitudes; this is why we expect that this IRI topside option is a good point of comparison. Table 2 points out that the α-Chapman topside profile is the best one compared to both the other topside profiles studied and the IRI-NeQuick topside model, by using both Swarm A and C and Swarm B-derived effective scale heights. With regard to the Swarm A and C data set, all the topside profiles (1a)–(1d), with the exception of the exponential one, provide a better accuracy than IRI-NeQuick. Instead, for the Swarm B data set, this holds true only for α-Chapman and exponential profiles. Moreover, all the topside profiles, with the exception of the exponential one, present worse performances for the Swarm B data set than for the Swarm A and C one. These results highlight that (a) α-Chapman, β-Chapman, and Epstein profiles can properly model the topside region immediately above the *F*2 layer peak, allowing a reliable description of the *F*2 layer shape; (b) in the upper topside region, by using a constant effective scale height for the entire topside region, α-Chapman, β-Chapman, and Epstein formulations no longer reliably represent its particular shape; (c) the exponential profile is the best one to model the upper part of the ionospheric topside region.

Table 2 shows also that each of the proposed topside profiles is characterized by a standard deviation lower than that associated to IRI-NeQuick, thus highlighting a higher precision of the proposed topside modeling method.

4. Conclusions

In the present paper an empirical method to model the lower part of the ionospheric topside profile has been presented, by using both Swarm's measured electron density values and IRI UP modeled *F*2 layer peak

characteristics. Effective scale height values have been calculated by using four different topside profiles and modeled as a function of *foF*2 and *hmF*2. A statistical analysis has been then carried out by comparing our modeled topside profiles with those measured by COSMIC satellites.

The main outcomes of this work are as follows.

1. Modeled effective scale heights as a function of normalized variables can be reliably considered constant in the lower topside region, from *hmF*2 to about 500 km of altitude. The consideration of this hypothesis for upper heights deserves more attention because of the increasingly importance of light ions and for other dynamics connected reasons.
2. Effective scale height median values, modeled by means of the proposed two-dimensional binning procedure as a function of only *foF*2 and *hmF*2, have the potentiality to be applied to ionosonde's derived measurements, or to ionospheric models, like IRI for example.
3. Swarm electron density measurements have the potentiality to be used to model the topside ionospheric region because of the particular geometry of their orbit. In addition, the IRI UP method turns out to be particularly suited to this task, being able to spatially describe the *F*2 layer peak characteristics, in regions where a good number of ionosonde stations are available. Thus, the proposed method can be used, with profit, in other regions besides Europe.
4. The α-Chapman topside profile presents the best performance compared to the β-Chapman, Epstein, and exponential topside profiles, and also compared to the IRI-NeQuick topside model, by using either Swarm A and C or Swarm B-derived effective scale heights.
5. All profiles, with the exception of the exponential one, provide worse performances for the Swarm B data set than for the Swarm A and C one. It seems that a topside profile consisting of an α-Chapman function, for the lower part of the region, and an exponential function, for the upper part of the region, could provide an improved description for the entire topside region.
6. All the proposed topside profiles are characterized by a standard deviation lower than that associated to IRI-NeQuick. This highlights a good precision of the proposed topside modeling method which then represents a valid Space Weather operational tool to reliably model the topside over the European region (from 15°W to 45°E in longitude and from 30°N to 60°N in latitude), once the *F*2 layer characteristics, namely, *foF*2 and *hmF*2, are known, either measured or modeled.

It is worth noting that effective scale height values have been modeled as a function of *foF*2 and *hmF*2, without explicating any local time/seasonal/solar or magnetic activity dependence, because these variations are implicitly embedded in *foF*2 and *hmF*2. With the growth of the electron density data set collected by Swarm, an attempt to explicit these dependencies could be done in the future.

The results here described highlight the potentiality of the α-Chapman function in describing the lower topside region and of the exponential function in describing the upper topside region. This suggests that the possibility to use a topside profile consisting of a sum of these two functions deserves to be thoroughly investigated.

Acknowledgments
The authors thank the European Space Agency for making Swarm data publicly available via the website https://earth.esa.int/web/guest/swarm/data-access and the Swedish Institute of Space Physics in the person of S. Buchert for the calibration of Swarm Langmuir Probe electron density data used in this work. This publication uses data from 14 ionospheric observatories in Europe, made available via the public access portal of the Digital Ionogram Database (http://ulcar.uml.edu/DIDBase/) of the Global Ionosphere Radio Observatory in Lowell, MA. The authors are indebted to the observatory directors and ionosonde operators for heavy investments of their time, effort, expertise, and funds needed to acquire and provide measurement data to academic research. The authors acknowledge the IRI team for developing and maintaining the IRI model and allowing the access to the Fortran code via the IRI's website (http://irimodel.org/). Thanks to the COSMIC/FORMOSAT-3 team to make freely available radio occultation data through the COSMIC Data Analysis and Archive Center (CDAAC, http://cdaac-www.cosmic.ucar.edu/cdaac/products.html).

References

Anthes, R. A., Ector, D., Hunt, D. C., Kuo, Y., Rocken, C., Schreiner, W. S., et al. (2008). The COSMIC/FORMOSAT-3 mission: Early results. *Bulletin of the American Meteorological Society*, *89*(3), 313–333. https://doi.org/10.1175/BAMS-89-3-313

Belehaki, A., Tsagouri, I., Kutiev, I., Marinov, P., & Fidanova, S. (2012). Upgrades to the topside sounders model assisted by Digisonde (TaD) and its validation at the topside ionosphere. *Journal of Space Weather and Space Climate*, *2*, A20. https://doi.org/10.1051/swsc/2012020

Bilitza, D. (1990). International Reference Ionosphere 1990, NSSDC/WDC-A-R&S 90-22

Bilitza, D. (2004). A correction for the IRI topside electron density model based on Alouette/ISIS topside sounder data. *Advances in Space Research*, *33*(6), 838–843. https://doi.org/10.1016/j.asr.2003.07.009

Bilitza, D. (2009). Evaluation of the IRI-2007 model options for the topside electron density. *Advances in Space Research*, *44*(6), 701–706. https://doi.org/10.1016/j.asr.2009.04.036

Bilitza, D., Altadill, D., Zhang, Y., Mertens, C., Truhlik, V., Richards, P., et al. (2014). The International Reference Ionosphere 2012—A model of international collaboration. *Journal of Space Weather and Space Climate*, *4*, A07. https://doi.org/10.1051/swsc/2014004

Bilitza, D., Reinisch, B. W., Radicella, S. M., Pulinets, S., Gulyaeva, T., & Triskova, L. (2006). Improvements of the International Reference Ionosphere model for the topside electron density profile. *Radio Science*, *41*, RS5S15. https://doi.org/10.1029/2005RS003370

Chapman, S. (1931). The absorption and dissociative or ionizing effect of monochromatic radiation in an atmosphere on a rotating Earth. *Proceedings of the Physical Society of London*, *43*(1), 26–45.

Chu, Y. H., Su, C. L., & Ko, H. T. (2010). A global survey of COSMIC ionospheric peak electron density and its height: A comparison with ground-based ionosonde measurements. *Advances in Space Research*, *46*(4), 431–439. https://doi.org/10.1016/j.asr.2009.10.014

Coisson, P., Radicella, S. M., Leitinger, R., & Nava, B. (2006). Topside electron density in IRI and NeQuick: Features and limitations. *Advances in Space Research*, *37*(5), 937–942. https://doi.org/10.1016/j.asr.2005.09.015

Fonda, C., Coisson, P., Nava, B., & Radicella, S. M. (2005). Comparison of analytical functions used to describe topside electron density profiles with satellite data. *Annals of Geophysics*, *48*(3). https://doi.org/10.4401/ag-3213

Friis-Christensen, E., Lühr, H., & Hulot, G. (2006). Swarm: A constellation to study the Earth's magnetic field. *Earth, Planets and Space*, *58*(4), 351–358. https://doi.org/10.1186/BF03351933

Galkin, I. A., & B. W. Reinisch (2008). The new ARTIST 5 for all digisondes, ionosonde network advisory group bulletin 69 (8 pp.). Retrieved from http://www.ips.gov.au/IPSHosted/INAG/web-69/2008/artist5-inag.pdf

Garcia-Fernandez, M., Hernandez-Pajares, M., Juan, J. M., & Sanz, J. (2003). Improvement of ionospheric electron density estimation with GPSMET occultations using Abel inversion and VTEC information. *Journal of Geophysical Research*, *108*(A9), 1338. https://doi.org/10.1029/2003JA009952

Habarulema, J. B., Katamzi, Z. T., & Yizengaw, E. (2014). A simultaneous study of ionospheric parameters derived from FORMOSAT-3/COSMIC, GRACE, and CHAMP missions over middle, low, and equatorial latitudes: Comparison with ionosonde data. *Journal of Geophysical Research: Space Physics*, *119*, 7732–7744. https://doi.org/10.1002/2014JA020192

Haji, G. A., & Romans, L. J. (1998). Ionospheric electron density profiles obtained with the global positioning system: Results from the GPS/MET experiment. *Radio Science*, *33*(1), 175–190. https://doi.org/10.1029/97RS03183

Hargreaves, J. K. (1992). *The solar-terrestrial environment*. New York: Cambridge University Press.

Huang, X., & Reinisch, B. W. (2001). Vertical electron content from ionograms in real time. *Radio Science*, *36*(2), 335–342. https://doi.org/10.1029/1999RS002409

Kitanidis, P. K. (1997). *Introduction to geostatistics: Application to hydrogeology*. Cambridge: Cambridge University Press.

Klobuchar, J. A., & Kunches, J. M. (2000). Eye on the ionosphere: The spatial variability of ionospheric range delay. *GPS Solutions*, *3*(3), 70–74. https://doi.org/10.1007/PL00012808

Knudsen, D. J., Burchill, J. K., Buchert, S. C., Eriksson, A. I., Gill, R., Wahlund, J. E., et al. (2017). Thermal ion imagers and Langmuir probes in the Swarm electric field instruments. *Journal of Geophysical Research: Space Physics*, *122*, 2655–2673. https://doi.org/10.1002/2016JA022571

Krankowski, A., Zakharenkova, I., Krypiak-Gregorczyk, A., Shagimuratov, I. I., & Wielgosz, P. (2011). Ionospheric electron density observed by FORMOSAT-3/COSMIC over the European region and validated by ionosonde data. *Journal of Geodesy*, *85*(12), 949–964. https://doi.org/10.1007/s00190-011-0481-z

Kutiev, I. S., & Marinov, P. G. (2007). Topside sounder model of scale height and transition height characteristics of the ionosphere. *Advances in Space Research*, *39*(5), 759–766. https://doi.org/10.1016/j.asr.2006.06.013

Kutiev, I. S., Marinov, P. G., & Watanabe, S. (2006). Model of topside ionosphere scale height based on topside sounder data. *Advances in Space Research*, *37*(5), 943–950. https://doi.org/10.1016/j.asr.2005.11.021

Lei, J., Syndergaard, S., Burns, A. G., Solomon, S. C., Wang, W., Zeng, Z., et al. (2007). Comparison of COSMIC ionospheric measurements with ground-based observations and model predictions: Preliminary results. *Journal of Geophysical Research*, *112*, A07308. https://doi.org/10.1029/2006JA012240

Liu, L., Huang, H., Chen, Y., Le, H., Ning, B., Wan, W., & Zhang, H. (2014). Deriving the effective scale height in the topside ionosphere based on ionosonde and satellite in situ observations. *Journal of Geophysical Research: Space Physics*, *119*, 8472–8482. https://doi.org/10.1002/2014JA020505

Liu, L., Le, H., Wan, W., Sulzer, M. P., Lei, J., & Zhang, M.-L. (2007). An analysis of the scale heights in the lower topside ionosphere based on the Arecibo incoherent scatter radar measurements. *Journal of Geophysical Research*, *112*, A06307. https://doi.org/10.1029/2007JA012250

Liu, L., Wan, W., Zhang, M.-L., Ning, B., Zhang, S.-R., & Holt, J. M. (2007). Variations of topside ionospheric scale height over Millstone Hill during the 30-day incoherent scatter radar experiment. *Annales Geophysicae*, *25*(9), 2019–2027. https://doi.org/10.5194/angeo-25-2019-2007

Liu, R. Y., Smith, P. A., & King, J. W. (1983). A new solar index which leads to improved *foF2* predictions using the CCIR Atlas. *Telecommunication Journal*, *50*, 408–414.

Luan, X., Liu, L., Wan, W., Lei, J., Zhang, S.-R., Holt, J. M., & Sulzer, M. P. (2006). A study of the shape of topside electron density profile derived from incoherent scatter radar measurements over Arecibo and Millstone Hill. *Radio Science*, *41*, RS4006. https://doi.org/10.1029/2005RS003367

Nava, B., Coisson, P., & Radicella, S. M. (2008). A new version of the NeQuick ionosphere electron density model. *Journal of Atmospheric and Solar - Terrestrial Physics*, *70*(15), 1856–1862. https://doi.org/10.1016/j.jastp.2008.01.015

Nsumei, P., Reinisch, B. W., Huang, X., & Bilitza, D. (2012). New Vary-Chap profile of the topside ionosphere electron density distribution for use with the IRI model and the GIRO real time data. *Radio Science*, *47*, RS0L16. https://doi.org/10.1029/2012RS004989

Olivares-Pulido, G., Hernandez-Pajares, M., Aragon-Angel, A., & Garcia-Rigo, A. (2016). A linear scale height Chapman model supported by GNSS occultation measurements. *Journal of Geophysical Research: Space Physics*, *121*, 7932–7940. https://doi.org/10.1002/2016JA022337

Pezzopane, M., & Scotto, C. (2005). The INGV software for the automatic scaling of foF2 and MUF(3000)F2 from ionograms: A performance comparison with ARTIST 4.01 from Rome data. *Journal of Atmospheric and Solar - Terrestrial Physics*, *67*(12), 1063–1073.

Pezzopane, M., & Scotto, C. (2007). The automatic scaling of critical frequency *foF2* and MUF(3000)*F2*: A comparison between Autoscala and ARTIST 4.5 on Rome data. *Radio Science*, *42*, RS4003. https://doi.org/10.1029/2006RS003581

Pezzopane, M., & Scotto, C. (2010). Highlighting the *F2* trace on an ionogram to improve Autoscala performance. *Computers & Geosciences*, *36*(9), 1168–1177. https://doi.org/10.1016/j.cageo.2010.01.010

Pezzopane, M., Scotto, C., Tomasik, L., & Krasheninnikov, I. (2010). Autoscala: An aid for different ionosondes. *Acta Geophysica*, *58*(3), 513–526. https://doi.org/10.2478/s11600-009-0038-1

Pignalberi, A., Pezzopane, M., Rizzi, R., & Galkin, I. (2018a). Effective solar indices for ionospheric modeling: A review and a proposal for a real-time regional IRI. *Surveys in Geophysics*, *39*(1), 125–167. https://doi.org/10.1007/s10712-017-9438-y

Pignalberi, A., Pezzopane, M., Rizzi, R., & Galkin, I. (2018b). Correction to: Effective solar indices for ionospheric modeling: A review and a proposal for a real-time regional IRI. *Surveys in Geophysics*, *39*(1), 169–169. https://doi.org/10.1007/s10712-017-9453-z

Pignalberi, A., Pezzopane, M., Tozzi, R., De Michelis, P., & Coco, I. (2016). Comparison between IRI and preliminar Swarm Langmuir probe measurements during the St. Patrick storm period. *Earth, Planets and Space*, *68*(1), 93. https://doi.org/10.1186/s40623-016-0466-5

Radicella, S. M., & Leitinger, R. (2001). The evolution of the DGR approach to model electron density profiles. *Advances in Space Research*, *27*(1), 35–40. https://doi.org/10.1016/S0273-1177(00)00138-1

Rawer, K. (1988). Synthesis of ionospheric electron density profiles with Epstein functions. *Advances in Space Research*, *8*(4), 191–199. https://doi.org/10.1016/0273-1177(88)90239-6

Reinisch, B. W., & Galkin, I. A. (2011). Global ionospheric radio observatory (GIRO). *Earth, Planets and Space*, *63*(4), 377–381. https://doi.org/10.5047/eps.2011.03.001

Reinisch, B. W., & Huang, X. (1983). Automatic calculation of electron density profiles from digital ionograms: 3. Processing of bottomside ionograms. *Radio Science*, *18*(3), 477–492.

Reinisch, B. W., Huang, X., Belehaki, A., Shi, J. K., Zhang, M. L., & Ilma, R. (2004). Modeling the IRI topside profile using scale heights from ground-based ionosonde measurements. *Advances in Space Research*, *34*(9), 2026–2031. https://doi.org/10.1016/j.asr.2004.06.012

Reinisch, B. W., Nsumei, P., Huang, X., & Bilitza, D. K. (2007). Modeling the *F*2 topside and plasmasphere for IRI using IMAGE/RPI and ISIS data. *Advances in Space Research*, *39*(5), 731–738. https://doi.org/10.1016/j.asr.2006.05.032

Rishbeth, H., & Garriott, O. (1969). *Introduction to ionospheric physics, International geophysics series* (Vol. 14). New York: Academic Press.

Schreiner, W. S., Sokolovskiy, S. V., Rocken, C., & Hunt, D. C. (1999). Analysis and validation of GPS/MET radio occultation data in the ionosphere. *Radio Science*, *34*(4), 949–966. https://doi.org/10.1029/1999RS900034

Scotto, C., & Pezzopane, M. (2008a). A method for automatic scaling of sporadic E layers from ionograms. *Radio Science*, *42*, RS2012. https://doi.org/10.1029/2006RS003461

Scotto, C., & Pezzopane, M. (2008b). Removing multiple reflections from the *F*2 layer to improve Autoscala performance. *Journal of Atmospheric and Solar - Terrestrial Physics*, *70*(15), 1929–1934. https://doi.org/10.1016/j.jastp.2008.05.012

Stankov, S. M., & Jakowski, N. (2006). Topside ionospheric scale height analysis and modelling based on radio occultation measurements. *Journal of Atmospheric and Solar - Terrestrial Physics*, *68*(2), 134–162. https://doi.org/10.1016/j.jastp.2005.10.003

Stankov, S. M., Jakowski, N., Heise, S., Muhtarov, P., Kutiev, I., & Warnant, R. (2003). A new method for reconstruction of the vertical electron density distribution in the upper ionosphere and plasmasphere. *Journal of Geophysical Research*, *108*(A5), 1164. https://doi.org/10.1029/2002JA009570

Třísková, L., Truhlík, V., & Šmilauer, J. (2006). An empirical topside electron density model for calculation of absolute ion densities in IRI. *Advances in Space Research*, *37*(5), 928–934. https://doi.org/10.1016/j.asr.2005.09.013

Tulasi Ram, S., Su, S.-Y., Liu, C. H., Reinisch, B. W., & McKinnell, L.-A. (2009). Topside ionospheric effective scale height (H_T) derived with ROCSAT-1 and ground-based ionosonde observations at equatorial and midlatitude stations. *Journal of Geophysical Research*, *114*, A10309. https://doi.org/10.1029/2009JA014485

Venkatesh, K., Rama Rao, P. V. S., & Fagundes, P. R. (2014). The role of altitudinal variation of scale height in determining the topside electron density profile over equatorial and low latitude sectors. *Journal of Atmospheric and Solar - Terrestrial Physics*, *121*, 72–82. https://doi.org/10.1016/j.jastp.2014.10.006

Venkatesh, K., Rama Rao, P. V. S., Saranya, P. L., Prasad, D. S. V. V. D., & Niranjan, K. (2011). Vertical electron density and topside effective scale height (H_T) variations over the Indian equatorial and low latitude stations. *Annales Geophysicae*, *29*(10), 1861–1872. https://doi.org/10.5194/angeo-29-1861-2011

Verhulst, T., & Stankov, S. M. (2014). Evaluation of ionospheric profilers using topside sounding data. *Radio Science*, *49*, 181–195. https://doi.org/10.1002/2013RS005263

Verhulst, T., & Stankov, S. M. (2015). Ionospheric specification with analytical profilers: Evidences of non-chapman electron density distribution in the upper ionosphere. *Advances in Space Research*, *55*(8), 2058–2069. https://doi.org/10.1016/j.asr.2014.10.017

Wang, S., Huang, S., & Fang, H. (2015a). Topside ionospheric VARY-chap scale height retrieved from the COSMIC/FORMOSAT-3 data at midlatitudes. *Advances in Space Research*, *56*(5), 893–899. https://doi.org/10.1016/j.asr.2015.04.021

Wang, S., Huang, S., & Fang, H. (2015b). New method for deriving the topside ionospheric Vary-Chap scale height. *Radio Science*, *50*, 866–875. https://doi.org/10.1002/2015RS005724

Wright, J. W. (1960). A model of the F region above $h_{max}F2$. *Journal of Geophysical Research*, *65*(1), 185–191. https://doi.org/10.1029/JZ065i001p00185

Wu, M. J., Guo, P., Fu, N. F., Xu, T. L., Xu, X. S., Jin, H. L., & Hu, X. G. (2016). Topside correction of IRI by global modeling of ionospheric scale height using COSMIC radio occultation data. *Journal of Geophysical Research: Space Physics*, *121*, 5675–5692. https://doi.org/10.1002/2016JA022785

Wu, X., Hu, H., Gong, X., Zhang, X., & Wang, X. (2009). Analysis of inversion errors of ionospheric radio occultation. *GPS Solutions*, *13*(3), 231–239. https://doi.org/10.1007/s10291-008-0116-x

Xu, T. L., Jin, H. L., Xu, X., Guo, P., Wang, Y. B., & Ping, J. S. (2013). Statistic analysis of the ionospheric topside scale height based on COSMIC RO measurements. *Journal of Atmospheric and Solar - Terrestrial Physics*, *104*, 29–38. https://doi.org/10.1016/j.jastp.2013.07.012

Yue, X., Schreiner, W. S., Lei, J., Sokolovskiy, S. V., Rocken, C., Hunt, D. C., & Kuo, Y. H. (2010). Error analysis of Abel retrieved electron density profiles from radio occultation measurements. *Annales Geophysicae*, *28*(1), 217–222. https://doi.org/10.5194/angeo-28-217-2010

Yue, X., Wan, W., Liu, L., & Mao, T. (2007). Statistical analysis on spatial correlation of ionospheric day-to-day variability by using GPS and incoherent scatter radar observations. *Annales Geophysicae*, *25*(8), 1815–1825. https://doi.org/10.5194/angeo-25-1815-2007

Zhang, M. L., Radicella, S. M., Kersley, I., & Pulinets, S. A. (2002). Results of the modeling of the topside electron density profile using the Chapman and Epstein functions. *Advances in Space Research*, *29*(6), 871–876. https://doi.org/10.1016/S0273-1177(02)00053-4

Zhu, J., Zhao, B., Wan, W., Ning, B., & Zhang, S. (2015). A new topside profiler based on Alouette/ISIS topside sounding. *Advances in Space Research*, *5*(10), 2080–2090. https://doi.org/10.1016/j.asr.2015.08.008